

Current Transport in Carbon Nanotube Transistors

(Invited Paper)

Mahdi Pourfath and Siegfried Selberherr

Institute for Microelectronics, TU Wien, 1040 Vienna, Austria

Email: {pourfath|selberherr}@iue.tuwien.ac.at

Abstract—Carbon nanotubes (CNTs) have been studied in recent years due to their exceptional electronic, opto-electronic, and mechanical properties. To explore the physics of carbon nanotube field-effect transistors (CNT-FETs) self-consistent quantum mechanical simulations have been performed. The performance of carbon nanotube-based transistors is analyzed numerically, employing the non-equilibrium Green's function formalism. Electron-phonon interaction parameters, such as electron-phonon coupling strength and phonon energy, strongly depend on the chirality and the diameter of the carbon nanotube. The steady-state and the dynamic response of carbon nanotube based transistors are studied for a wide range of electron-phonon interaction parameters.

I. INTRODUCTION

Novel structures and materials such as multiple gate MOS-FETs, carbon nanotube field-effect transistors (CNT-FETs), and molecular based transistors, are expected to be introduced to meet the requirements for scaling [1]. CNTs can be considered as a graphene sheet which has been wrapped into a tube. The way the graphene sheet is wrapped is represented by a pair of indices (n, m) called the chiral vector. The integers n and m denote the number of unit vectors along two directions in the honeycomb crystal lattice of graphene. If $m = 0$, the CNT is called *zigzag*. If $n = m$, the CNT is called *armchair*. Otherwise, it is called *chiral*. CNTs with $n - m = 3$ are metals, otherwise they are semiconductors [2]. Semiconducting CNTs can be used as channels for transistors [3], and metallic CNTs can serve as interconnect wires [4].

CNT-FETs have been considered in recent years as potential alternatives to CMOS devices due to their excellent electronic properties [5, 6]. Some of the interesting electronic properties of CNTs are quasi-ballistic carrier transport [7], suppression of short-channel effects due to one-dimensional electron transport [8, 9], and nearly symmetric structure of the conduction and valence bands [10], which is advantageous for complementary circuits. Moreover, owing to excellent optical properties of CNTs, an all-CNT electronic and opto-electronic devices can be envisioned. The direct band-gap and the tunability of the band-gap with the CNT diameter renders them as suitable candidates for opto-electronic devices, especially for infra-red (IR) applications [11, 12] due to the relatively narrow band gap.

The non-equilibrium Green's function (NEGF) method has been successfully utilized to investigate the characteristics of nano-scale silicon transistors [13–15], CNT-FETs [16–24], and molecular devices [25–30]. In this work we discuss the NEGF formalism to study quantum transport in CNT-FETs.

The outline of the paper is as follows. In Section II, the NEGF formalism is briefly described. The implementation of this method for CNT-FETs is presented in Section III. The electron-phonon interaction parameters of a CNT depend on the chiral vector, which implies that many different parameter values exist. In Section IV the device response is studied for a wide range of electron-phonon interaction parameters. After a brief discussion in Section V conclusions are presented in Section VI.

II. NON-EQUILIBRIUM GREEN'S FUNCTION FORMALISM

The NEGF formalism initiated by Schwinger, Kadanoff, and Baym allows to study the time evolution of a many-particle quantum system. Knowing the single-particle Green's functions of a given system, one may evaluate single-particle quantities such as carrier density and current. The many-particle information about the system is cast into self-energies, which are part of the equations of motion for the Green's functions. A perturbation expansion of the Green's functions is the key to approximate the self-energies. Green's functions enable a powerful technique to evaluate the properties of a many-body system both in thermodynamic equilibrium and non-equilibrium situations.

Four types of Green's functions are defined as the non-equilibrium statistical ensemble averages of the single particle correlation operator [31]. The greater Green's function $G^>$ and the lesser Green's function $G^<$ deal with the statistics of carriers. The retarded Green's function G^R and the advanced Green's function G^A describe the dynamics of carriers.

$$\begin{aligned} G^>(1, 2) &= -i\hbar^{-1}\langle\hat{\psi}(1)\hat{\psi}^\dagger(2)\rangle \\ G^<(1, 2) &= +i\hbar^{-1}\langle\hat{\psi}^\dagger(2)\hat{\psi}(1)\rangle \\ G^R(1, 2) &= \theta(t_1 - t_2)[G^>(1, 2) - G^<(1, 2)] \\ G^A(1, 2) &= \theta(t_2 - t_1)[G^<(1, 2) - G^>(1, 2)] \end{aligned} \quad (1)$$

The abbreviation $1 \equiv (\mathbf{r}_1, t_1)$ is used, $\langle \dots \rangle$ is the statistical average with respect to the density operator, $\theta(t)$ is the unit step function, $\hat{\psi}^\dagger(\mathbf{r}_1, t_1)$ and $\hat{\psi}(\mathbf{r}_1, t_1)$ are the field operators creating or destroying a particle at point (\mathbf{r}_1, t_1) in space-time, respectively. The Green's functions are all correlation functions. For example, $G^>$ relates the field operator $\hat{\psi}$ of the particle at point (\mathbf{r}_1, t_1) in space-time to the conjugate field operator $\hat{\psi}^\dagger$ at another point (\mathbf{r}_2, t_2) .

Under steady state condition the Green's functions depend only on time differences. One usually Fourier transforms the

time difference coordinate, $\tau = t_1 - t_2$, to energy. For example, the lesser Green's function is transformed as $G^<(1, 2) \equiv G^<(\mathbf{r}_1, \mathbf{r}_2; E) = \int (d\tau/\hbar) e^{iE\tau/\hbar} G^<(\mathbf{r}_1, \mathbf{r}_2; \tau)$.

Under steady-state condition the equation of motion for the Green's functions can be written as [32]:

$$[E - H] G^{R,A}(1, 2) - \int d3 \Sigma^{R,A}(1, 3) G^{r,a}(3, 2) = \delta_{1,2} \quad (2)$$

$$G^{\lessgtr}(1, 2) = \int d3 \int d4 G^R(1, 3) \Sigma^{\lessgtr}(3, 4) G^A(4, 2) \quad (3)$$

where H is the single-particle Hamiltonian operator, and Σ^R , $\Sigma^<$, and $\Sigma^>$ are the retarded, lesser, and greater self-energies, respectively.

III. IMPLEMENTATION

This section describes the implementation of the outlined NEGF formalism for the numerical analysis of CNT-FET. Fig. 1 shows the structure of the simulated device. A tight-

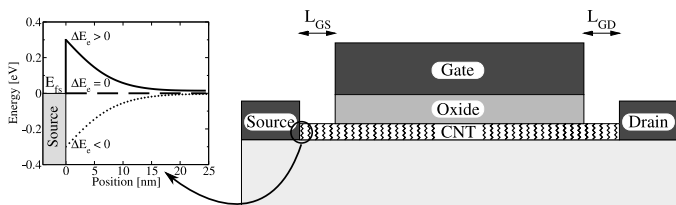


Fig. 1. Cross section of the investigated CNT based transistor and the band-edge profile at the source sided metal-CNT interface. Depending on the work function difference between metal and CNT, a positive, zero, or negative barrier height for electrons or holes can be achieved.

binding Hamiltonian is used to describe transport phenomena in CNT-FETs. The self-energy due to electron-phonon interactions are studied next.

A. Tight-Binding Hamiltonian

In Graphene three σ bonds hybridize in an sp^2 configuration, whereas the other $2p_z$ orbital, which is perpendicular to the graphene layer, forms π covalent bonds. The π energy bands are predominantly determining the solid state properties of graphene. Similar considerations hold for CNTs. We use a nearest-neighbor tight-binding π -bond model [33]. Each atom in an sp^2 -coordinated CNT has three nearest neighbors, located $a_{cc} = 1.42 \text{ \AA}$ away. The band-structure consists of π -orbitals only, with the hopping parameter $t = V_{pp\pi} \approx -2.7 \text{ eV}$ and zero on-site potential.

The tight-binding Hamiltonian matrix for a $(n, 0)$ zigzag CNT, shown in Fig. 2-a, can be written as [33]

$$\underline{H} = \begin{pmatrix} \underline{U}_1 & \underline{t}_1 & & & & & \\ \underline{t}_1^\dagger & \underline{U}_2 & & & & & \\ & \underline{t}_2^\dagger & \underline{U}_3 & & & & \\ & & \underline{t}_1 & \underline{U}_4 & & & \\ & & & \underline{t}_2 & \underline{U}_5 & & \\ & & & & & \ddots & \ddots \end{pmatrix} \quad (4)$$

where the underlined quantities denote matrices. We assume that the electrostatic potential shifts the on-site potential.

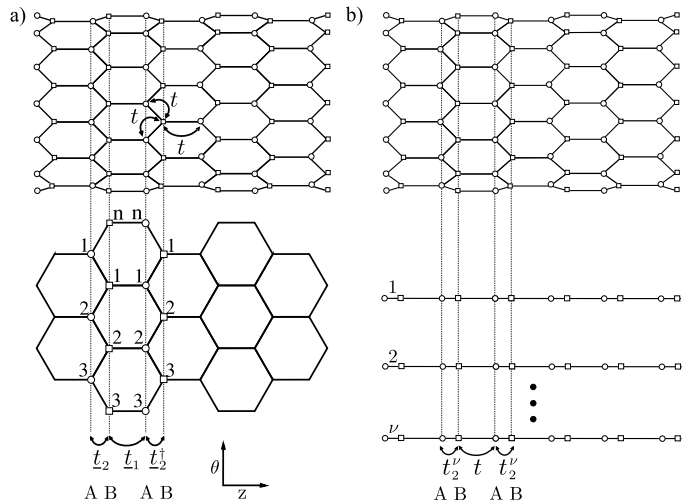


Fig. 2. Layer layout of a $(n, 0)$ zigzag CNT. a) The coupling matrices between layers are denoted by t_1 and t_2 , where t_1 is a diagonal matrix and t_2 includes off-diagonal elements. b) The corresponding one-dimensional chain, in mode space, with two sites per unit cell with hopping parameters t and $t'_2 = 2t \cos(\pi\nu/n)$.

Therefore, U_i is a diagonal matrix which represents the electrostatic potential energy in the i th circumferential ring of carbon atoms. Equal electrostatic potential for all carbon atoms within a ring is assumed, therefore $U_i = U_i \underline{I}$. The first and second kind of interaction matrix between the neighboring rings are denoted by t_1 and t_2 . Only the nearest neighbor interaction between carbon atoms is considered. The coupling matrix between layer 2 and layer 3 is diagonal, $t_1 = t \underline{I}$, where t is the hopping parameter. However, the coupling matrix between layer 1 and layer 2 is given by

$$\underline{t}_2 = \begin{pmatrix} t & & t \\ t & t & \\ & t & t \\ & & & \ddots \end{pmatrix} \quad (5)$$

The eigen vectors of the matrix \underline{t}_2 represent plane waves around the circumference of the CNT with the quantized wave-vectors $k_\nu = 2\pi\nu/\sqrt{3}a_{cc}n$, where $\nu = 1, 2, \dots, n$ [33], and the eigen values $2t \cos(\pi\nu/n)$. By transforming from real space into eigen mode space [34], the subbands become decoupled and the Hamiltonian can be written as $\underline{H} = \sum_\nu \underline{H}^\nu$, where \underline{H}^ν , the Hamiltonian of the subband ν , is given by

$$\underline{H}^\nu = \begin{pmatrix} U_1^\nu & t_1^\nu & & & & & \\ t_1^\nu & U_2^\nu & t_2^\nu & & & & \\ & t_2^\nu & U_3^\nu & t_1^\nu & & & \\ & & t_1^\nu & U_4^\nu & t_2^\nu & & \\ & & & t_2^\nu & U_5^\nu & & \\ & & & & & \ddots & \ddots \end{pmatrix}, \quad (6)$$

where $U_i^\nu = U_i$, $t_1^\nu = t$, and $t_2^\nu = 2t \cos(\pi\nu/n)$ [23, 33]. The one-dimensional tight-binding Hamiltonian \underline{H}^ν describes a chain with two sites per unit cell with on-site potential U_i^ν and hopping parameters t and t_2^ν , see Fig. 2-b.

B. Electron-Phonon Self-Energies

Because in the CNT two degrees of freedom are confined, an electron can only be scattered forward or backward in the axial direction, preserving or changing the sign of the band-velocity, respectively. We assume bias conditions for which the first subband predominantly contributes to the total current and only intra-subband intra-valley transitions have to be considered.

A linear dispersion relation for acoustic phonons is assumed, $\omega_{q,\lambda} \approx v_\lambda|q|$, where v_λ is the acoustic phonon velocity and λ is the phonon polarization. For optical phonons the energy is assumed to be independent of the phonon wave-vector $\omega_{q,\lambda} \approx \omega_{\text{OP},\lambda} = \text{const}$. Similarly, the matrix elements of electron-phonon interaction [35] can be approximated as $M_{q,\lambda} \approx M_\lambda^{\text{AP}}|q|$ for acoustic phonons and $M_{q,\lambda} \approx M_\lambda^{\text{OP}} = \text{const}$ for optical phonons. The interaction of electrons with optical phonons is inelastic. Assuming that the electron-phonon interaction occurs locally [36] the self-energies can be written as

$$\Sigma_{\text{inel}}^{<,\nu}(E) = \sum_\lambda D_{\text{inel},\lambda} \times [(N_\lambda + 1)G^{<,\nu}(E + \hbar\omega_\lambda) + N_\lambda G^{<,\nu}(E - \hbar\omega_\lambda)] \quad (7)$$

$$\Sigma_{\text{inel}}^{>,\nu}(E) = \sum_\lambda D_{\text{inel},\lambda} \times [(N_\lambda + 1)G^{>,\nu}(E - \hbar\omega_\lambda) + N_\lambda G^{>,\nu}(E + \hbar\omega_\lambda)] \quad (8)$$

where N_λ is the phonon occupation number which is given by the Bose-Einstein distribution function. The electron-phonon interaction strength is given by

$$D_{\text{inel},\lambda} = \frac{\hbar|M_\lambda^{\text{OP}}|^2}{2nm_c\omega_\lambda} \quad (9)$$

where m_c is the mass of a carbon atom. The first term in (7) corresponds to the emission of a phonon by the de-excitation of an electron and the second term corresponds to the excitation of an electron by the absorption of a phonon. Interaction with acoustic phonons can be regarded as elastic scattering, $E \pm \hbar\omega_\lambda \approx E$, and the approximation $N_\lambda \approx N_\lambda + 1 \approx k_B T / \hbar v_\lambda$ can be used. Based on this approximation, the self-energies for acoustic phonon interaction simplify to

$$\Sigma_{\text{el}}^{\lessgtr,\nu}(E) = D_{\text{el}}^\nu G^{\lessgtr,\nu}(E) \quad (10)$$

$$D_{\text{el},\lambda} = \frac{k_B T |M_\lambda^{\text{AP}}|^2}{nm_c v_\lambda} \quad (11)$$

The self-energy due to electron-phonon interaction comprises the contributions of elastic and inelastic scattering mechanisms, $\Sigma_{\text{e-ph}}^\nu = \Sigma_{\text{el}}^\nu + \Sigma_{\text{inel}}^\nu$. The transport equations must be iterated to achieve convergence of the electron-phonon self-energies, resulting in a self-consistent Born approximation.

C. Self-Consistent Simulations

To solve transport equations numerically they need to be discretized in both the spatial and the energy domain. The carrier concentration at some node l of the spatial grid and

the current density at the edge between the nodes l and $l + 1$ are given by

$$n_l = -4i \sum_\nu \int \frac{dE}{2\pi} G_{l,l}^{<,\nu}(E) \quad (12)$$

$$j_{l,l+1} = \frac{4q}{\hbar} \sum_\nu \int \frac{dE}{2\pi} 2\Re\{G_{l,l+1}^{<,\nu}(E)t_{l+1,l}^\nu\} \quad (13)$$

where the factor 4 is due to the spin and band degeneracy.

For an accurate analysis it is essential to solve the coupled system of transport equations and the Poisson equation self-consistently [30]. The convergence of the self-consistent iteration is a critical issue. To achieve convergence, fine resonances at some energies in (12) have to be resolved accurately. For that purpose an adaptive method for selecting the energy grid is essential [37].

IV. THE EFFECT OF ELECTRON-PHONON INTERACTION

The electron-phonon coupling strength and the phonon energy depend on the chirality and the diameter of the CNT [35]. In this section the device response is studied for a wide range of electron-phonon interaction parameters.

A. Electron-Phonon Coupling Strength

Fig. 3-a shows the ballisticity as a function of the electron-phonon coupling strength. The ballisticity is defined as $I_{\text{Sc}}/I_{\text{Bl}}$, the ratio of the on-current in the presence of electron-phonon interaction to the current in the ballistic case [38].

The left part of Fig. 3-b illustrates an electron losing its kinetic energy by emitting a phonon. The electron will be scattered either forward or backward. In the case of backward scattering the electron faces a thick barrier near the source contact and will be reflected with high probability, such that its momentum will again be directed towards the drain contact.

Elastic scattering conserves the energy of carriers, but the current decreases due to elastic back-scattering of carriers. Fig. 4-a shows that for elastic scattering the source and drain current spectra are symmetric. As the electron-phonon coupling strength increases, resonances in the current spectrum are washed out and the total current decreases due to elastic back-scattering. In the case of inelastic scattering, carriers acquiring enough kinetic energy can emit a phonon and scatter

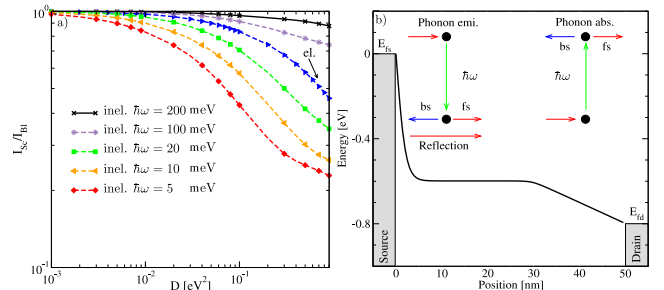


Fig. 3. a) Ballisticity versus electron-phonon coupling strength for a CNT of 50 nm length. Results for both elastic and inelastic scattering with different phonon energies are shown. The operating point is $V_G = V_D = 1$ V. b) Sketch of phonon emission and absorption processes in the channel.

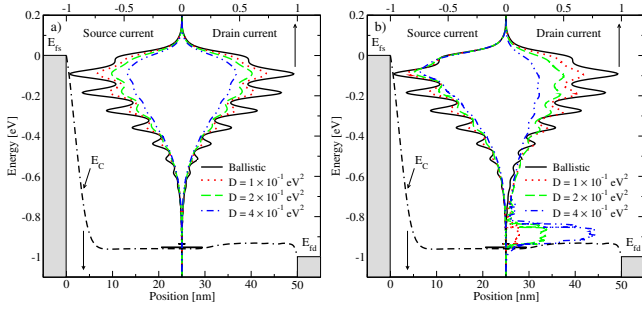


Fig. 4. The spectra of the source and drain currents. a) The effect of elastic phonon scattering with different coupling strengths is shown. b) The effect of inelastic phonon scattering with different coupling strengths is shown. The phonon energy is $\hbar\omega = 100$ meV.

into lower energy states. Therefore, as shown in Fig. 4-b, the source and drain current spectra are not symmetric. As the coupling strength increases more electrons are scattered into lower energy states.

B. Phonon Energy

Figure 5-a shows the dependence of the ballisticity with respect to the phonon energy. With increasing phonon energy the effect of phonon scattering on the current is reduced, because scattered electrons lose more kinetic energy and the probability for traveling back to the source contact decreases. The considerable decrease of ballisticity for low energy phonons is due to the phonon absorption process. The right part of Fig. 3-b shows an electron absorbing energy from a phonon and scattering into a higher energy state. In this case, the probability for arriving at the source contact increases. This process can severely reduce the total current.

Fig. 5-b separately shows the effects of the phonon emission and absorption processes on the ballisticity. As the phonon energy decreases, the phonon occupation number increases exponentially, and the self-energy contributions of these two components increase. However, due to the higher probability for back-scattering of electrons in the case of phonon absorption, this component reduces the total current more effectively than the phonon emission process does.

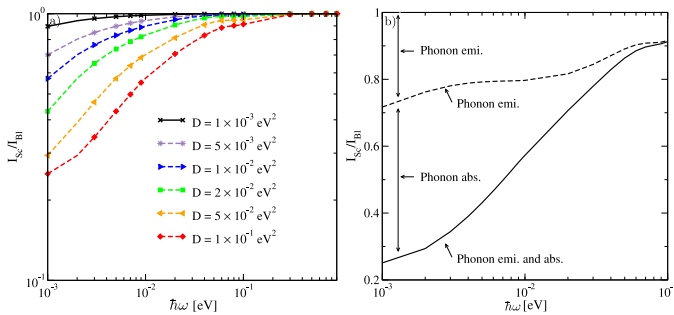


Fig. 5. a) Ballisticity versus phonon energy for a CNT of 50 nm length. Results for inelastic scattering with different electron-phonon couplings are shown. $V_G = V_D = 1$ V. b) Ballisticity versus phonon energy with $D = 10^{-1}$ eV² at the bias point $V_G = V_D = 1$ V. The contributions due to phonon absorption and emission are shown.

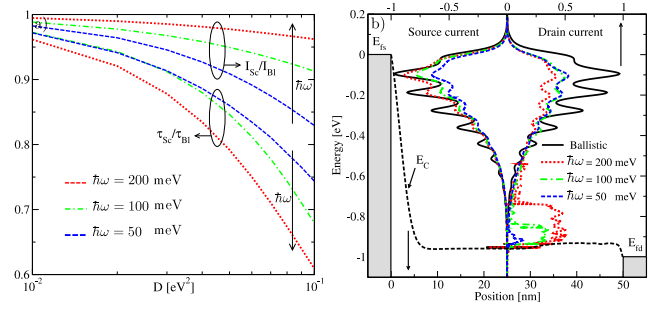


Fig. 6. a) The ratio of the gate-delay time in the ballistic case to that in the presence of electron-phonon interaction. For comparison, the ratio I_{Sc}/I_{BI} is also shown. b) The spectra of the source and drain currents. The effect of inelastic scattering with different phonon energies is shown. The electron-phonon coupling strength is $D = 2 \times 10^{-1}$ eV². A considerable increase of the electron population close to the conduction band-edge as the phonon energy increases is visible.

C. Switching Response

To illustrate the effect of electron-phonon interaction on the dynamic response of the device, the gate-delay time defined as $\tau = (Q_{on} - Q_{off})/I_{on}$ [39] is considered, where the quasi static approximation is assumed. It has been shown that the quasi static approximation for CNT based transistors is justified for frequencies below THz [40].

Fig. 6-a shows the ratio of the gate-delay time in the ballistic case to that in the presence of electron-phonon interaction, τ_{BI}/τ_{Sc} , as a function of the electron-phonon coupling strength. As the phonon energy increases the gate-delay time increases. This behavior can be attributed to the average electron velocity in the channel, which is high for ballistic electrons and low for electrons scattered to lower energy states.

Fig. 6-b shows the spectra of the source and drain currents for different inelastic phonon energies. Electrons can emit a single phonon or a couple of phonons to reach lower energy states. The probability of multiple phonon emissions decreases as the number of interactions increases. Therefore, as the phonon energy increases, the occupation of electrons at lower energy states increases.

As shown in Fig. 6-b, the electron population close to the conduction band-edge considerably increases as the phonon energy increases. Therefore, as the phonon energy increases the mean velocity of electrons decreases and the carrier concentration in the channel increases (Fig. 7). The increased charge in the channel results in an increased gate-delay time.

D. Diffusive Limit

All the above discussed results were obtained for a device with a CNT length of 50 nm. In the case of ballistic transport the current is independent of the device length, but in the presence of scattering it decreases as the device length increases. Fig. 8-a shows the ballisticity as a function of the CNT length in the presence of elastic and inelastic electron-phonon interaction. An artificially large value for the electron-phonon coupling strength and a small value for the phonon

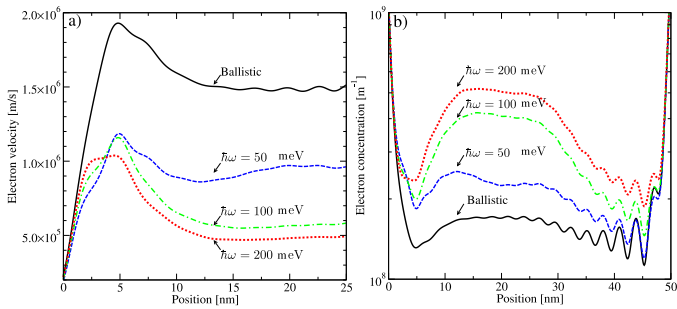


Fig. 7. a) The profile of the electron velocity near the source contact. b) The profile of the electron concentration along the device. The results for the ballistic case and for electron-phonon interaction are shown. As the phonon energy increases the electrons scatter to lower energy states. Therefore, the electron velocity decreases and the carrier concentration increases. The electron-phonon coupling strength is $D = 10^{-1} \text{ eV}^2$ and the bias point is $V_G = V_D = 1 \text{ V}$.

energy is chosen to simulate the diffusive limit (see Fig. 8-b). In this case the current is expected to be inversely proportional to the device length according to Ohm's law.

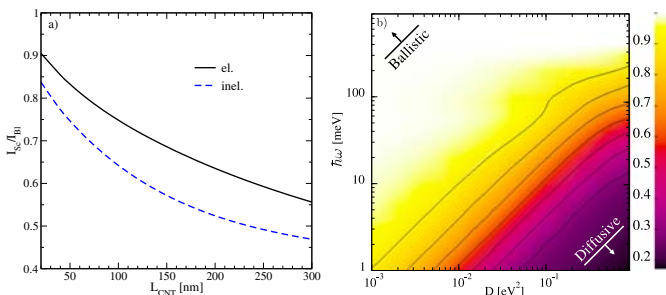


Fig. 8. a) Ballistic transport parameter versus CNT length. The electron-phonon coupling strength for both elastic and inelastic scattering is $D = 10^{-1} \text{ eV}^2$, and $\hbar\omega = 25 \text{ meV}$ for inelastic scattering. These scattering parameters simulate the diffusive regime. In this case the ballisticity is inversely proportional to the device length [41]. b) Ballisticity as a function of the electron-phonon coupling strength and phonon energy for inelastic scattering. The scale of the ballisticity is shown in the side bar. The regions of ballistic and diffusive transport are shown. As the strength of the electron-phonon interaction increases transport of carriers deviates from the ballistic limit and becomes more diffusive.

V. DISCUSSION

In general the electron-phonon interaction parameters depend on the diameter and the chirality of the CNT [35]. CNTs with a diameter $d_{\text{CNT}} > 2 \text{ nm}$ have a band gap $E_G < 0.4 \text{ eV}$, which render them unsuitable as channel for transistors. Since the fabrication of devices with a diameter $d_{\text{CNT}} < 1 \text{ nm}$ is very difficult, we limit our study to zigzag CNTs with diameters in the range of $d_{\text{CNT}} = 1 - 2 \text{ nm}$.

Scattering with acoustic phonons is treated as an elastic process. The electron-phonon coupling is also weak for acoustic phonons ($D_{\text{AP}} < 10^{-3} \text{ eV}^2$), which implies that elastic back-scattering of carriers is weak. Inelastic scattering is induced by optical (OP), radial breathing mode (RBM), and K-point phonons [10, 43]. Considering the class of CNTs discussed above, energies of these phonons are $\hbar\omega_{\text{OP}} \approx 200 \text{ meV}$, $\hbar\omega_{\text{RBM}} \approx 25 \text{ meV}$, and

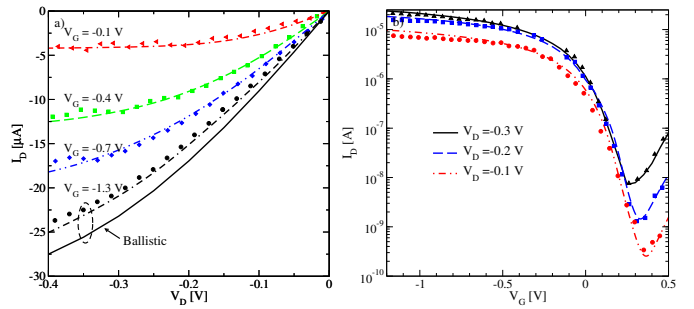


Fig. 9. Comparison of the simulation results and experimental data for the a) output and b) transfer characteristics. Lines show the simulation results and symbols show experimental data. The result for $V_G = -1.3 \text{ V}$ is compared with the ballistic limit. Experimental data have been adopted from [42].

$\hbar\omega_{\text{K}_1} \approx 160 \text{ meV}$ and $\hbar\omega_{\text{K}_2} \approx 180 \text{ meV}$ [38, 43]. The corresponding coupling coefficients are $D_{\text{OP}} \approx 40 \times 10^{-3} \text{ eV}^2$, $D_{\text{RBM}} \approx 10^{-3} \text{ eV}^2$, and $D_{\text{K}_1} \approx 10^{-4} \text{ eV}^2$, and $D_{\text{K}_2} \approx 10^{-3} \text{ eV}^2$ [38].

As discussed in Section IV-B, high energy phonons such as OP and K-point phonons reduce the on-current only weakly, but can increase the gate-delay time considerably due to charge pileup in the channel. Low energy phonons such as the RBM phonon can reduce the on-current more effectively, but have a weaker effect on the gate-delay time. However, due to strong coupling, scattering processes are mostly due to electron-phonon interaction with high energy phonons. Therefore, at room temperature the on-current of short CNT-FETs can be close to the ballistic limit [42] (see Fig. 9), whereas the gate-delay time can be significantly below that limit [44–46].

The intrinsic (without parasitic capacitances) gate-delay time for the ballistic case can be approximated as $\tau \approx 1.7 \text{ ps}/\mu\text{m}$, or equivalently $f_T \approx 100 \text{ GHz}/\mu\text{m}$ [39]. The highest reported intrinsic cutoff frequency for a device with a length of 300 nm is $f_T \approx 30 \text{ GHz}$ [47], which is far below the ballistic limit. Inelastic electron-phonon interaction with high energy phonon has to be considered to explain the results.

VI. CONCLUSION

The coupled system of transport and Poisson equations was solved self-consistently. A tight-binding Hamiltonian is used to describe transport phenomena in CNT-FETs. Employing the described model, both the static and dynamic response of CNT-FETs was investigated. The effect of electron-phonon interaction on the device characteristics is discussed in detail. In agreement with experimental data, our results indicate that at room temperature electron phonon interaction affects the steady-state current of CNT-FETs only weakly, whereas the switching response of such devices can be significantly affected.

ACKNOWLEDGMENT

This work was supported by funds from the Austrian Science Foundation (FWF), contract I79-N16.

REFERENCES

- [1] "International Technology Roadmap for Semiconductors - 2007 Edition," Semiconductor Industry Association, Tech. Rep. [Online]. Available: <http://public.itrs.net>
- [2] R. Saito, T. Takeya, T. Kimura, G. Dresselhaus, and M. S. Dresselhaus, "Raman Intensity of Single-Wall Carbon Nanotubes," *Phys. Rev. B*, vol. 57, no. 7, pp. 4145–4153, 1998.
- [3] R. Martel, T. Schmidt, H. Shea, T. Hertel, and P. Avouris, "Single- and Multi-Wall Carbon Nanotube Field-Effect Transistors," *Appl. Phys. Lett.*, vol. 73, no. 17, pp. 2447–2449, 1998.
- [4] W. Hoenlein, F. Kreupl, G. Duesberg, A. Graham, M. Liebau, R. Seidel, and E. Unger, "Carbon Nanotube Applications in Microelectronics," *IEEE Trans. Comp. Packag. Technol.*, vol. 27, no. 4, pp. 629–634, 2004.
- [5] J. Appenzeller, "Carbon Nanotubes for High-Performance Electronics—Progress and Prospects," *Proc. IEEE*, vol. 96, no. 2, pp. 201–211, 2008.
- [6] P. Avouris, Z. Chen, and V. Perebeinos, "Carbon Based Electronics," *Nature Nanotechnology*, vol. 2, no. 10, pp. 605–615, 2007.
- [7] A. Javey, J. Guo, Q. Wang, M. Lundstrom, and H. Dai, "Ballistic Carbon Nanotube Field-Effect Transistors," *Nature (London)*, vol. 424, no. 6949, pp. 654–657, 2003.
- [8] R. V. Seidel, A. P. Graham, J. Kretz, B. Rajasekharan, G. S. Duesberg, M. Liebau, E. Unger, F. Kreupl, and W. Hoenlein, "Sub-20 nm Short Channel Carbon Nanotube Transistors," *Nano Lett.*, vol. 5, no. 1, pp. 147–150, 2005.
- [9] J.-Y. Park, "Carbon Nanotube Field-Effect Transistor with a Carbon Nanotube Gate Electrode," *Nanotechnology*, vol. 18, no. 9, p. 095202, 2007.
- [10] R. Saito, G. Dresselhaus, and M. Dresselhaus, *Physical Properties of Carbon Nanotubes*. London: Imperial College Press, 1998.
- [11] M. Freitag, J. Chen, J. Tersoff, J. Tsang, Q. Fu, J. Liu, and P. Avouris, "Mobile Ambipolar Domain in Carbon-Nanotube Infrared Emitters," *Phys. Rev. Lett.*, vol. 93, p. 076803, 2004.
- [12] M. Freitag, Y. Martin, J. Misewich, R. Martel, and P. Avouris, "Photoconductivity of Single Carbon Nanotubes," *Nano Lett.*, vol. 3, no. 8, pp. 1067–1071, 2003.
- [13] A. Svizhenko, M. P. Anantram, T. R. Govindan, B. Biegel, and R. Venugopal, "Two-Dimensional Quantum Mechanical Modeling of Nanotransistors," *J. Appl. Phys.*, vol. 91, no. 4, pp. 2343–2354, 2002.
- [14] A. Svizhenko and M. P. Anantram, "Role of Scattering in Nanotransistors," *IEEE Trans. Electron Devices*, vol. 50, no. 6, pp. 1459–1466, 2003.
- [15] R. Venugopal, M. Paulsson, S. Goasguen, S. Datta, and M. S. Lundstrom, "A Simple Quantum Mechanical Treatment of Scattering in Nanoscale Transistors," *J. Appl. Phys.*, vol. 93, no. 9, pp. 5613–5625, 2003.
- [16] M. B. Nardelli, "Electronic Transport in Extended Systems: Application to Carbon Nanotubes," *Phys. Rev. B*, vol. 60, no. 11, pp. 7828–7833, 1999.
- [17] J. Taylor, H. Guo, and J. Wang, "Ab Initio Modeling of Quantum Transport Properties of Molecular Electronic Devices," *Phys. Rev. B*, vol. 63, p. 245407, 2001.
- [18] J. J. Palacios, A. J. P. Jimenez, E. Louis, E. SanFabio, and J. Verges, "First-Principles Phase-Coherent Transport in Metallic Nanotubes with Realistic Contacts," *Phys. Rev. Lett.*, vol. 90, p. 106801, 2003.
- [19] Y. Xue and M. A. Ratner, "Schottky Barriers at Metal-Finite Semiconducting Carbon Nanotube Interfaces," *Appl. Phys. Lett.*, vol. 83, no. 12, pp. 2429–2431, 2003.
- [20] J. Guo, "A Quantum-Mechanical Treatment of Phonon Scattering in Carbon Nanotube Transistors," *J. Appl. Phys.*, vol. 98, p. 063519, 2005.
- [21] J. Guo, S. Hassan, A. Javey, G. Bosman, and M. Lundstrom, "Assessment of High-Frequency Performance Potential of Carbon Nanotube Transistors," *IEEE Trans. Nanotechnol.*, vol. 4, no. 6, pp. 715–721, 2005.
- [22] A. Svizhenko, M. P. Anantram, and T. R. Govindan, "Ballistic Transport and Electrostatics in Metallic Carbon Nanotubes," *IEEE Trans. Nanotechnol.*, vol. 4, no. 5, pp. 557–562, 2005.
- [23] A. Svizhenko and M. Anantram, "Effect of Scattering and Contacts on Current and Electrostatics in Carbon Nanotubes," *Phys. Rev. B*, vol. 72, p. 085430, 2005.
- [24] M. Pourfath and H. Kosina, "The Effect of Phonon Scattering on the Switching Response of Carbon Nanotube FETs," *Nanotechnology*, vol. 18, pp. 424036–6, 2007.
- [25] W. Tian, S. Datta, S. Hong, R. Reifengerger, J. I. Henderson, and C. P. Kubiak, "Conductance Spectra of Molecular Wires," *J. Chem. Phys.*, vol. 109, no. 7, pp. 2874–2882, 1998.
- [26] P. S. Damle, A. W. Ghosh, and S. Datta, "Unified Description of Molecular Conduction: From Molecules to Metallic Wires," *Phys. Rev. B*, vol. 64, p. 201403, 2001.
- [27] J. M. Seminario, L. E. Cordova, and P. A. Derosa, "An Ab Initio Approach to the Calculation of Current-Voltage Characteristics of Programmable Molecular Devices," *Proc. IEEE*, vol. 91, no. 11, pp. 1958–1975, 2003.
- [28] M. Galperin, A. Nitzan, S. Sek, and M. Majda, "Asymmetric Electron Transmission across Asymmetric Alkanethiol Bilayer Junctions," *J. Electroanal. Chem.*, vol. 550–551, no. 1, pp. 337–350, 2003.
- [29] Y. Xue and M. A. Ratner, "End Group Effect on Electrical Transport through Individual Molecules: A Microscopic Study," *Phys. Rev. B*, vol. 69, p. 085403, 2004.
- [30] A. W. Ghosh, T. Rakshit, and S. Datta, "Gating of a Molecular Transistor: Electrostatic and Conformational," *Nano Lett.*, vol. 4, no. 4, pp. 565–568, 2004.
- [31] G. D. Mahan, *Many-Particle Physics*, 2nd ed., ser. Physics of Solids and Liquids. New York: Plenum Press, 1990.
- [32] S. Datta, *Electronic Transport in Mesoscopic Systems*. New York: Cambridge University Press, 1995.
- [33] J. Guo, S. Datta, M. Lundstrom, and M. Anantram, "Multi-Scale Modeling of Carbon Nanotube Transistors," *The International Journal of Multiscale Computational Engineering*, vol. 2, no. 2, pp. 257–278, 2004.
- [34] R. Venugopal, Z. Ren, S. Datta, M. Lundstrom, and D. Jovanovic, "Simulating Quantum Transport in Nanoscale Transistors: Real Versus Mode-Space Approaches," *J. Appl. Phys.*, vol. 92, no. 7, pp. 3730–3739, 2002.
- [35] V. N. Popov and P. Lambin, "Intraband Electron-Phonon Scattering in Single-Walled Carbon Nanotubes," *Phys. Rev. B*, vol. 74, p. 075415, 2006.
- [36] R. Lake and S. Datta, "Nonequilibrium Green's-Function Method Applied to Double-Barrier Resonant-Tunneling Diodes," *Phys. Rev. B*, vol. 45, no. 12, pp. 6670–6685, 1992.
- [37] M. Pourfath and H. Kosina, "A Fast and Stable Poisson-Schrödinger Solver for the Analysis of Carbon Nanotube Transistors," *J. Comp. Electronics*, vol. 5, no. 2-3, pp. 155–159, 2006.
- [38] S. O. Koswatta, S. Hasan, M. Lundstrom, M. P. Anantram, and D. E. Nikonov, "Ballisticities of Nanotube FETs: Role of Phonon Energy and Gate Bias," *Appl. Phys. Lett.*, vol. 89, p. 023125, 2006.
- [39] Y. Yoon, Y. Ouyang, and J. Guo, "Effect of Phonon Scattering on Intrinsic Delay and Cutoff Frequency of Carbon Nanotube FETs," *IEEE Trans. Electron Devices*, vol. 53, no. 10, pp. 2467–2470, 2006.
- [40] Y. Chen, Y. Ouyang, J. Guo, and T. X. Wu, "Time-Dependent Quantum Transport and Nonquasistatic Effects in Carbon Nanotube Transistors," *Appl. Phys. Lett.*, vol. 89, p. 203122, 2006.
- [41] M. Lundstrom, "Elementary Scattering Theory of the Si MOSFET," *IEEE Electron Device Lett.*, vol. 18, no. 7, pp. 361–363, 1997.
- [42] A. Javey, J. Guo, D. Farmer, Q. Wang, E. Yenilmez, R. Gordon, M. Lundstrom, and H. Dai, "Self-Aligned Ballistic Molecular Transistors and Electrically Parallel Nanotube Arrays," *Nano Lett.*, vol. 4, no. 7, pp. 1319–1322, 2004.
- [43] J. Park, S. Rosenblatt, Y. Yaish, V. Sazonova, H. Ustunel, S. Braig, T. Arias, P. Brouwer, and P. McEuen, "Electron-Phonon Scattering in Metallic Single-Walled Carbon Nanotubes," *Nano Lett.*, vol. 4, no. 3, pp. 517–520, 2004.
- [44] D. Singh, K. Jenkins, J. Appenzeller, D. Neumayer, A. Grill, and H.-S. P. Wong, "Frequency Response of Top-Gated Carbon Nanotube Field-Effect Transistors," *IEEE Trans. Nanotechnol.*, vol. 3, no. 3, pp. 383–387, 2004.
- [45] D. Frank and J. Appenzeller, "High-Frequency Response in Carbon Nanotube Field-Effect Transistors," *IEEE Electron Device Lett.*, vol. 25, no. 1, pp. 34–36, 2004.
- [46] X. Huo, M. Zhang, P. C. H. Chan, Q. Liang, and Z. K. Tang, "High Frequency S parameters Characterization of Back-Gate Carbon Nanotube Field-Effect Transistors," in *Intl. Electron Device Meet. Tech. Dig.* San Francisco: IEEE, 2004, pp. 691–694.
- [47] A. L. Louarn, F. Kapche, J.-M. Bethoux, H. Happy, G. Dambriane, V. Derycke, P. Chenevier, N. Izard, M. F. Goffman, and J. Bourgoin, "Intrinsic Current Gain Cutoff Frequency of 30 GHz with Carbon Nanotube Transistors," *Appl. Phys. Lett.*, vol. 90, p. 233108, 2007.